ESR study of the spin ladder with uniform Dzyaloshinskii-Moriya interaction

V. N. Glazkov,[1,2,*] M. Fayzullin,[3] Yu. Krasnikova,[1,2] G. Skoblin,[1,2,†] D. Schmidiger,[4] S. Mühlbauer,[4,‡] and A. Zheludev[4]

[1]*P. L. Kapitza Institute for Physical Problems RAS, Kosygin strasse 2, 119334 Moscow, Russia*

[2]*Moscow Institute of Physics and Technology, 141700 Dolgoprudny, Russia*

[3]*Institute for Physics, Kazan Federal University, 18 Kremlyovskaya strasse 18, 420008, Kazan, Russia*

[4]*Neutron Scattering and Magnetism, Laboratory for Solid State Physics, ETH Zürich, 8006 Zürich, Switzerland*

(Received 9 July 2015; revised manuscript received 28 August 2015; published 3 November 2015)

Evolution of the ESR absorption in a strong-leg spin ladder magnet $(C_7H_{10}N)_2CuBr_4$ (abbreviated as DIMPY) is studied from 300 K to 400 mK. Temperature dependence of the ESR relaxation follows a staircase of crossovers between different relaxation regimes. We argue that the main mechanism of ESR line broadening in DIMPY is uniform Dzyaloshinskii-Moriya interaction ($|\mathbf{D}| = 0.31$ K) with an effective longitudinal component along an exchange bond of Cu ions within the legs resulting from the low crystal symmetry of DIMPY and nontrivial orbital ordering. The same Dzyaloshinskii-Moriya interaction along with other weaker anisotropic spin-spin interactions results in the lifting of the triplet excitation degeneracy, revealed through the weak splitting of the ESR absorption at low temperatures.

DOI: 10.1103/PhysRevB.92.184403 PACS number(s): 75.10.Kt, 76.30.−v

I. INTRODUCTION

Low-dimensional magnets have been actively studied during the last decades both theoretically and experimentally. Spin ladder is one of the simplest models of the field that is just one step more complicated than the Heisenberg spin chain, the keystone of low-dimensional magnetism. Such a system consists of two chains forming the "legs" of the spin ladder, which are coupled by simple interchain coupling forming "rungs" of the ladder. The Hamiltonian of the single spin ladder with the equivalent positions along the ladder is

$$\mathcal{H} = J_{\text{leg}} \sum_i (\mathbf{S}_{1,i}\mathbf{S}_{1,i+1} + \mathbf{S}_{2,i}\mathbf{S}_{2,i+1}) + J_{\text{rung}} \sum_i \mathbf{S}_{1,i}\mathbf{S}_{2,i} + \mu_B \mathbf{H}\hat{g} \sum_{j,i} \mathbf{S}_{j,i} + \mathcal{H}_{\text{anis}}, \quad (1)$$

it includes Heisenberg exchange couplings J_{leg} and J_{rung}, Zeeman interaction (with usually anisotropic g tensor), and weak anisotropic spin-spin interactions $\mathcal{H}_{\text{anis}}$.

Independent of the ratio between the J_{leg} and J_{rung}, the excitation spectrum of the spin ladder is gapped, ground state is nonmagnetic, and excited states are $S = 1$ quasiparticles [1]. However, most of the experimentally available examples of the spin ladder systems are so-called strong-rung ladders with the dominating in-rung interaction J_{rung}. Strong-leg ladders remain a rarity in this family. An additional complication of the real systems is a presence of the anisotropic spin-spin interactions breaking the ideal symmetry of the Heisenberg model. Such interactions limit the excitation lifetime (to the point of total damping in some extreme cases [2]) and could lift degeneracy of the $S = 1$ states. Thus, estimation of such an interaction strength, and, ideally, the search for systems with a negligible anisotropic part of the Hamiltonian is an important quest when comparing real magnets with model predictions.

Adequate accounting for the effect of anisotropic interactions in a spin-gap magnet is also a challenge. This problem was addressed in a one-dimensional (1D) field theory model via bosonic [3] and fermionic [4] approaches and in an independently developed macroscopic model [5]. However, a reliable microscopic model remain a rarity (see, e.g., Ref. [6]): most of the real spin-gap magnets have a complicated network of the exchange couplings allowing far too numerous possibilities of the anisotropic interaction parameters. The adequate microscopic approaches are of particular interest in connection with a particular case of the effect of a uniform Dzyaloshinskii-Moriya interaction on the properties of a quantum magnet [7].

A recently found organometallic compound $(C_7H_{10}N)_2CuBr_4$, abbreviated DIMPY for short, is an example of the strong-leg ladder with very weak anisotropic interactions [8–11]. Presence of the energy gap in the excitation spectrum was revealed by magnetic susceptibility [8], specific heat [9], and magnetization [11,12] bulk measurements as well as by inelastic neutron scattering [9,10]. The energy gap was found [9] to be 0.33 meV, it can be closed by the magnetic field $\mu_0 H_{c1} \approx 3$ T, while the saturation field is much higher [12], $\mu_0 H_{\text{sat}} \approx 30$ T. The values of the exchange constants were determined from the DMRG fit of the measured inelastic neutron scattering spectra [11] and were found to be $J_{\text{leg}} = 1.42$ meV and $J_{\text{rung}} = 0.82$ meV. The magnetic field induced ordering is observed at very low temperatures ($T_N^{(\max)} \approx 300$ mK at $\mu_0 H \sim 15$ T) [11].

Electron spin resonance (ESR) spectroscopy is a powerful tool to probe for the weak anisotropic interactions in the magnetic systems. Inelastic neutron scattering experiments [10] have shown that DIMPY is an almost perfect realization of the Heisenberg spin ladder. The ESR technique allows much higher energy resolution (routinely resolved ESR linewidth of 100 Oe corresponds approximately to the energy resolution of 1 μeV) and thus allows us to probe possible effects of anisotropic interactions with high accuracy.

*glazkov@kapitza.ras.ru

†Current address: Quantum Device Physics Laboratory, Department of Microtechnology and Nanoscience, Chalmers University of Technology, SE-412 96 Göteborg, Sweden.

‡Current address: Heinz Maier-Leibnitz Zentrum (MLZ), Garching D-85748, Germany.

In the present paper we report results of the ESR study of low-energy spin dynamics in DIMPY in the temperature range from 400 mK to 300 K. We observe angular and temperature dependencies of the ESR linewidth at high temperatures which can be described as an effect of the uniform Dzyaloshinskii-Moriya (DM) interaction allowed by the lattice symmetry. At low temperatures we observe splitting of the ESR absorption line due to lifting of the triplet state degeneracy caused by interplay of DM interaction and weaker anisotropic interactions. Additionally we observe well resolved ESR absorption lines from the inequivalent ladders which allowed an upper estimate of interladder exchange interaction.

During the preparation of the paper we became aware of the high-field ESR study of DIMPY [13]. This study reports observation of the additional high-frequency ESR mode which became allowed due to the presence of DM coupling, thus supporting claims on the importance of the DM coupling to the physics of this compound.

II. SAMPLES AND EXPERIMENTAL DETAILS

Single crystals of nondeuterated DIMPY were grown from the solution by slow diffusion in a temperature gradient. Sample quality was checked by x-ray diffraction and magnetization measurements. Concentration of the paramagnetic defects estimated from the 500 mK magnetization curve is below 0.05%.

DIMPY belongs to the monoclinic space group $P2(1)/n$ with lattice parameters $a = 7.504$ Å, $b = 31.613$ Å, $c = 8.206$ Å, and the angle $\beta = 98.972^\circ$ [8]. As-grown crystals have a well developed plane orthogonal to the b axis and are elongated along the a direction.

ESR experiments were performed using a set of the home-made transmission-type ESR spectrometers at the frequencies 18–105 GHz. The lowest available temperature of 400 mK was obtained by a He-3 vapors pumping cryostat. At the measurements below 77 K the magnetic field was created by compact superconducting magnets. Typical nonuniformity of the magnetic field at the resonance conditions in our experiments is estimated as <5–20 Oe depending on the magnet used. High-temperature experiments were done with a resistive water-cooled magnet with the field nonuniformity about 5 Oe.

III. LATTICE SYMMETRY AND POSSIBLE ANISOTROPIC INTERACTIONS

A monoclinic unit cell of DIMPY includes four magnetic Cu^{2+} ions that belong to two spin ladders: two pairs of copper ions form rungs of the spin ladders, which are then reproduced by translations along the a axis. This results in the formation of two ladders differently oriented with respect to the crystal [10] (see Fig. 1).

Space symmetry of the DIMPY lattice includes an inversion center in the middle of each rung and a second order screw axis parallel to the crystallographic b direction that links different ladders.

These symmetries place strong restrictions on the possible microscopic anisotropic interactions in DIMPY despite the low crystallographic symmetry. First, all anisotropic interactions

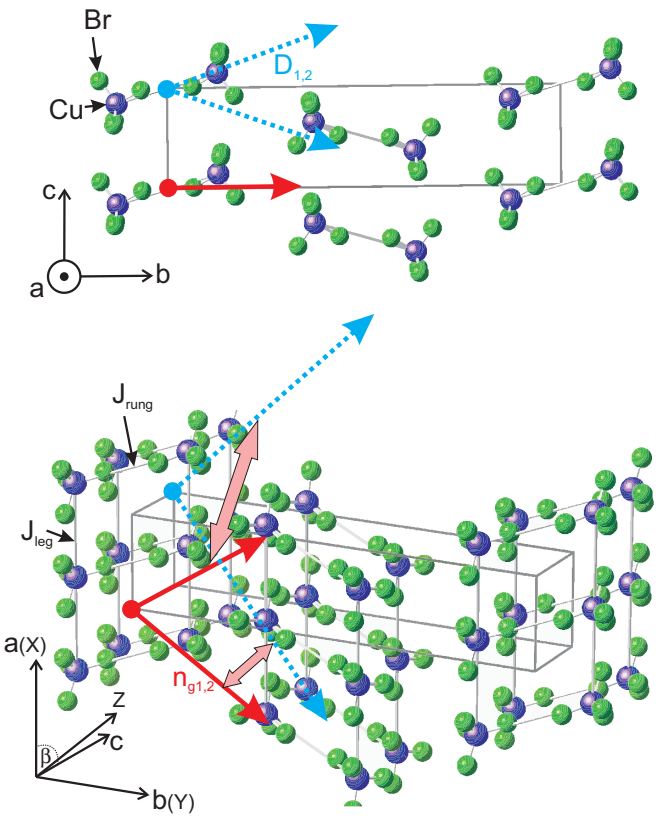

FIG. 1. (Color online) Crystallographic structure of DIMPY with two magnetically nonequivalent spin ladders. Only Cu and Br ions are shown along with the main exchange bonds J_{leg} and J_{rung}. Solid arrows (red) indicate directions of g tensor main axes for inequivalent ladders. Dashed arrows (blue) indicate directions of the Dzyaloshinskii-Moriya vectors for inequivalent ladders, as found from the data fit (see text). Broad double-headed arrows links the DM vector and g-tensor axis corresponding to the same ladder.

along the legs of the ladders should be uniform because of translational symmetry. Second, Dzyaloshinskii-Moriya antisymmetric interaction $\mathcal{H}_{DM} = \mathbf{D} \cdot [\mathbf{S}_1 \times \mathbf{S}_2]$ on the rungs is forbidden by the inversion symmetry. The same inversion symmetry requires that directions of the Dzyaloshinskii-Moriya vectors **D** have to be exactly opposite on the legs of the same ladder. Third, the inversion center on the rung of the ladder ensures that g tensor is always the same for the given spin ladder so there are no complications of anisotropic Zeeman splitting. Because of these symmetry restrictions there is no staggered component of the vector **D** for the single ladder.

The second order axis establishes relations between the g-tensor components and the Dzyaloshinskii-Moriya vector direction in different ladders. In particular, the effective g-factor values are the same for both ladders for the field applied parallel or orthogonal to this axis. Variation of the vector **D** direction in different ladders will be later accounted for explicitly in the linewidth analysis.

Note that antiparallel alignment of the DM vectors on the legs of the ladder does not allow us to use spin operator transformations of Ref. [7] which proves equivalence of the uniform DM coupling and shift in k space by wave vector $k = D/J$ for the *single* chain with uniform DM coupling.

Besides, the antisymmetric DM coupling symmetric anisotropic exchange (SAE) coupling is possible. SAE coupling can be written as $\mathcal{H}_{\rm SAE} = \sum_{\mu,\tau} J_{\mu\tau} S_1^{\mu} S_2^{\tau}$, where $J_{\mu\tau}$ are components of a symmetric exchange tensor $\hat{\mathbf{A}}$, which is usually constrained by condition ${\rm Tr} J_{\mu,\tau} = 0$. Symmetric interaction is allowed both on rungs and legs of the ladder. As we will demonstrate below, our observations point out that the Dzyaloshinskii-Moriya interaction is dominating anisotropic interaction in the case of DIMPY.

We neglect possible anisotropic interladder couplings in our analysis since the spin ladders in DIMPY are practically decoupled. Still, there is a possibility that anisotropic couplings between the equivalent ladders stacked in the c direction could be important as well: Cu-Cu distance in this direction is even less than the distance on the rungs (8.2 Å against 8.9 Å) and suppression of the Heisenberg exchange interaction in this direction is due to unfavorable mutual orientation of the electron orbitals of bromine ions mediating this superexchange route which could be less important for the anisotropic spin-spin interactions arising through involvement of differently oriented excited electron orbitals mixed with the ground state by spin-orbital interaction [14]. In the present work we neglect this possibility.

Thus, the main anisotropic interactions in DIMPY are really simple to analyze. They include anisotropic g tensor, which is the same for all magnetic ions of the given spin ladder, and the Dzyaloshinskii-Moriya interaction, which is uniform along the leg of the ladder, and the Dzyaloshinskii-Moriya vectors are exactly opposite on the legs of the given ladder.

IV. EXPERIMENTAL RESULTS

A. Angular dependence of the ESR absorption at 77 K

We have taken rotational patterns of ESR absorption for the magnetic field applied in different crystallographic planes. Because of monoclinic lattice symmetry care should be taken with consistent determination of the field direction with respect to the lattice axes. We use a crystallographic Cartesian basis with $X||a$, $Y||b$, and $Z||c^*$ for the direction description. Some of the measurements were done for the field applied or the rotation axis set at 45° from one Cartesian axis to another, these bisectrices of the Cartesian planes are denoted as $Y + X$, $Y - X$, $Y + Z$, and so on. Rotation patterns were taken for the field confined to (XY) and (XZ) planes and to the plane containing the Z axis and an $(Y - X)$ direction. All rotation patterns were taken for more than 180° angular sweeps.

Examples of absorption spectra and angular dependencies of the g factor are shown in Fig. 2. We observe one or two Lorentzian absorption lines. These absorption lines are clearly due to the different spin ladders: the ladders are equivalent with respect to the magnetic field for $\mathbf{H}||Y$ and $\mathbf{H} \perp Y$, and we observe single component absorption at these orientations. Anisotropy of the g factor is typical for the Cu^{2+} ion, the g factor varies from about 2.03 to 2.30 in agreements with powder ESR measurements of Ref. [15].

Angular dependence of the ESR linewidth was determined by fitting observed absorption spectra with a single Lorentzian line or with a sum of two Lorentzian lines (Fig. 2). Typical half-width at half-height at 77 K was around 50 Oe. Field

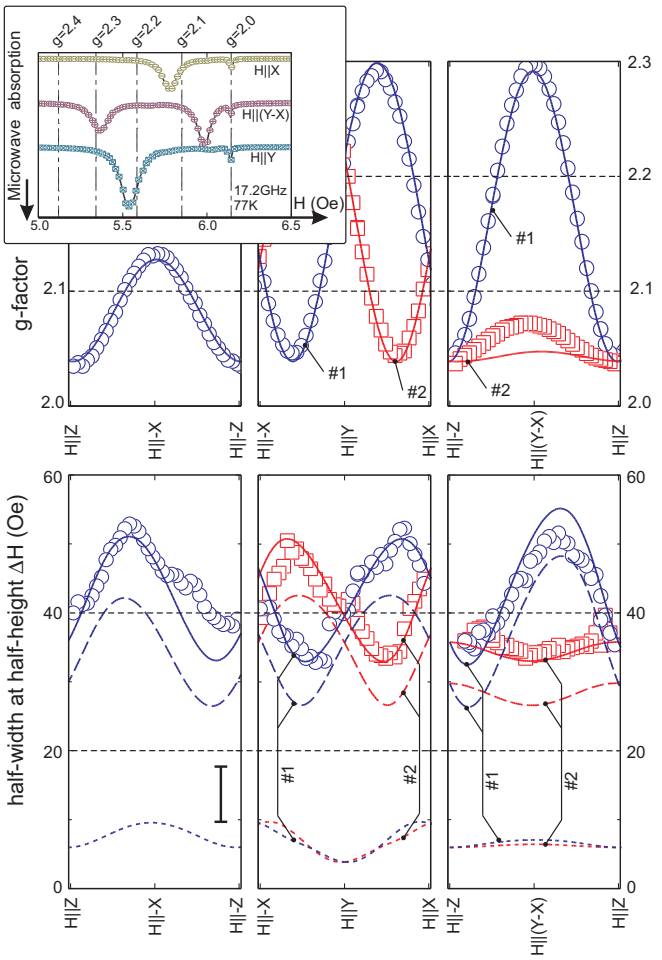

FIG. 2. (Color online) Inset: Example of ESR absorption spectra at representative orientations. Symbols: experimental data, curves: best fit with Lorentzian line shape, and vertical lines correspond to corresponding g-factor values. Narrow line with $g = 2.00$ (at 6.13 kOe) is a DPPH marker. Upper row: Angular dependence of the g factor at 77 K. Symbols: experimental data, curves: uniaxial g-tensor best fit (see text). Experimental error is about 0.1% and is within symbol size. Lower row: Angular dependence of the ESR linewidth at $f = 17.2$ GHz, $T = 77$ K (half-width at half-height). Vertical bar in left panel shows typical error bar size (double error). Curves: model description (see text), solid lines show full linewidth, dashed and dotted lines show contributions due to DM and SAE interactions, respectively. Marks "1" and "2" indicate contributions corresponding to the same ladder.

inhomogeneity in the used magnet and uncertainties of the fit procedure limit accuracy of the linewidth determination to about 5 Oe, however angular dependence is clearly present. We were able to cross check our results at certain selected orientations on a commercial Bruker X-band (9.3 GHz) spectrometer and we have found that X-band data are in agreement with our results.

B. Low-temperature ESR

Low temperature (below 77 K) ESR absorption was measured at certain fixed field directions: for the field applied parallel to the symmetry axis $\mathbf{H}||Y$ and for the field $\mathbf{H}||(X + Y)$

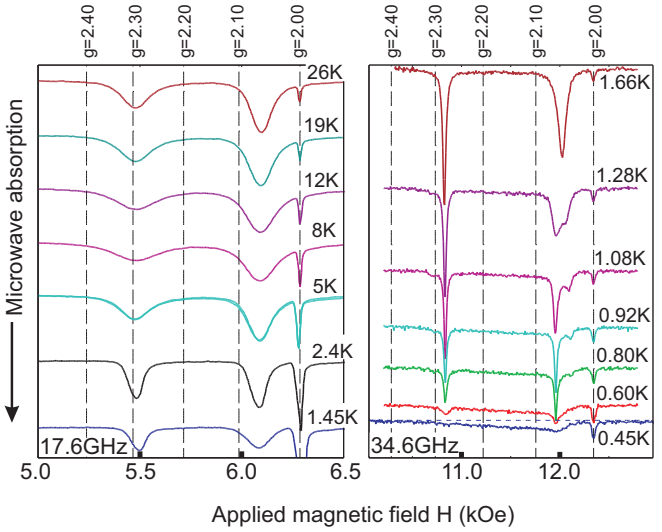

FIG. 3. (Color online) ESR absorption spectra at low temperatures, $\mathbf{H}||(X+Y)$. Vertical dashed lines mark resonance fields corresponding to the shown g-factor values. Horizontal dashed line at the 0.45 K curve is a guide to the eye at zero-absorption level. Narrow absorption line at $g = 2.00$ is a DPPH marker.

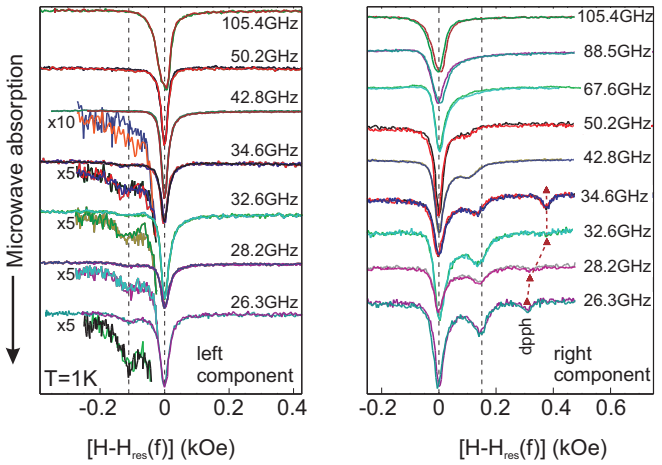

FIG. 4. (Color online) ESR absorption spectra at the temperature $T \approx 1$ K at different frequencies, $\mathbf{H}||(X+Y)$. All spectra are shifted along the field axis to fit positions of the main absorption subcomponents. Left panel: Left absorption component ($g \approx 2.28$), weak absorption subcomponent is magnified by a factor of 5 or 10 for better presentation. Right panel: Right absorption component ($g \approx 2.05$). Vertical dashed lines mark positions of the absorption subcomponent at lowest frequency. Triangles on the right panel mark positions of the DPPH marker absorption ($g = 2.00$).

direction (i.e., canted by 45° from the Y axis towards the X axis). In the first case both ladders are equivalently oriented with respect to the magnetic field, while the later case corresponds to the maximal difference of the ladders' effective g factors as evidenced by 77 K measurements.

As expected, we observe single-component ESR absorption for $\mathbf{H}||Y$ and two resolved ESR signals from different ladders for the canted sample. Temperature evolution of the ESR absorption spectra is qualitatively similar in both cases (Fig. 3). Below 10 K the ESR absorption intensity freezes down due to the presence of the energy gap. The ESR signal continues to lose intensity down to 450 mK and almost vanishes at this temperature. The lowest temperature (450 mK) ESR absorption includes broad powderlike absorption spectrum probably related to the distorted surface of the sample.

We did not observed any additional absorption signals which could be related to the formation of the field induced ordered phase above the critical field to appear at the lowest temperature of 450 mK in the fields up to 10 T at the frequencies of 26–35 GHz. This is in agreement with the known phase diagram of DIMPY [11] demonstrating that highest temperature of the transition into the ordered state is about 300 mK.

Additional splitting of the ESR absorption lines was observed around 1 K (Fig. 4), resonance fields of the split subcomponents differ by approximately 150 Oe. This splitting was observed at various frequencies, it was most pronounced on the high-field component of the canted sample ESR absorption spectra. One of the split subcomponents is much weaker than the other and freezes out faster on cooling. Remarkably, mutual orientation of the weaker and stronger subcomponents is different for the low-field and high-field components. We did not observe resolved splitting for the $\mathbf{H}||Y$ orientation, instead a weak peak of the linewidth was observed around the same temperature of 1 K probably indicating unresolved splitting.

At low temperatures intensities of all components follow exponential law $I \propto \exp(-\Delta/T)$ (Fig. 5). Energy gap for the weaker subcomponents is larger than that for the main subcomponents. By taking temperature dependencies of the ESR absorption at different frequencies we were able to determine the values of the energy gaps at several frequencies revealing dependence of the activation energy from the resonance field (Fig. 5).

C. ESR linewidth evolution from 300 K to 400 mK

Temperature evolution of the ESR linewidth was measured from room temperature down to 400 mK (Fig. 6). The temperature dependence is qualitatively similar in all orientations and demonstrates strongly nonmonotonous behavior. At high temperatures (above 90 K) linewidth strongly increases with heating rising from about 50 Oe at 77 K to about 300 Oe at 300 K. On cooling below 77 K linewidth again increases reaching maximum at temperature $T_{max} = 9.0 \pm 0.2$ K. Temperature of the maximum is the same for all orientations, while linewidth value at the maximum varies from 90 to 140 Oe, both of the extreme values being observed in the orientation of maximal splitting $\mathbf{H}||(X+Y)$ for different components of ESR absorption. Below T_{max} linewidth again decreases reaching a minimal value of about 10 Oe (observed at $\mathbf{H}||Y$) at 2 K, which is most likely limited by the field inhomogeneity in our setup. On cooling below 2 K a peak in the linewidth is observed around 1 K. The peak is most pronounced for the high-field component in the orientation of maximal splitting of the ESR absorption components, peak position coincides with the temperature of subcomponents appearance. A similar but less pronounced peak is observed for $\mathbf{H}||Y$. High-g component

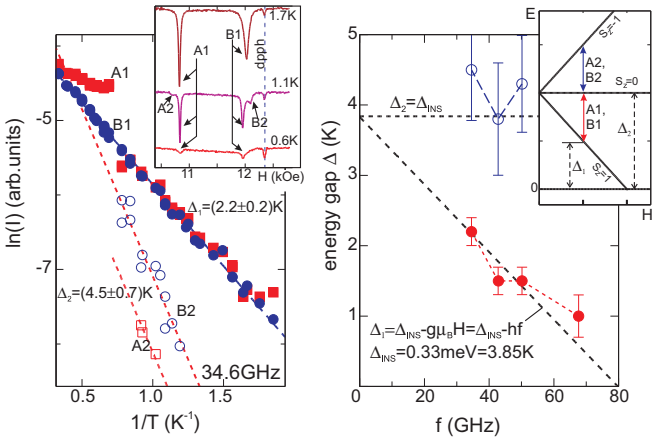

FIG. 5. (Color online) Left panel: Temperature dependence of the ESR intensity below 1 K at $f = 34.6$ GHz, $\mathbf{H}||(X+Y)$. Inset: Examples of ESR absorption and ESR components and subcomponents notations. Symbols: experimental data, dashed lines: fits with thermoactivation law $I \propto \exp(-\Delta/T)$. Right panel: Dependence of the determined activation gaps for different spectral subcomponents. Filled symbols: intense A1 and B1 subcomponents, open symbols: weak A2 and B2 subcomponents. Lines: parameters-free model dependence calculated with the zero-field gap value Δ_{INS} known from the inelastic neutron scattering experiments [9,10]. Inset: Scheme of the energy levels of a spin-gap magnet in a magnetic field. Solid vertical arrows show transitions corresponding to the observed ESR absorption, dashed vertical arrows mark activation gaps for these transitions.

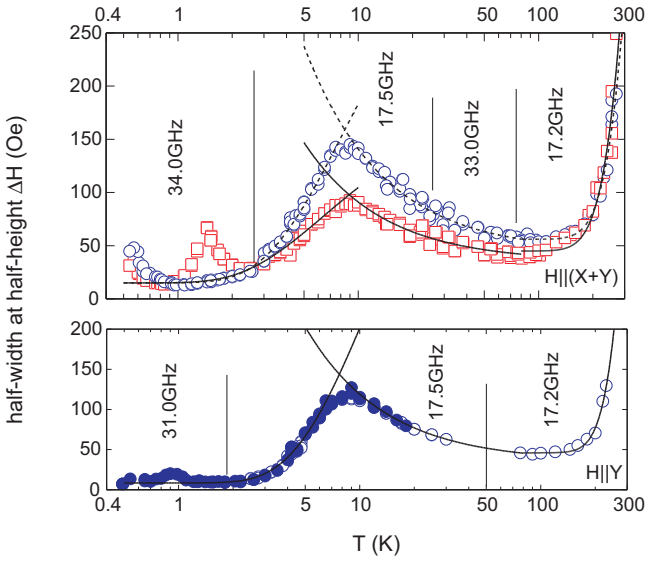

FIG. 6. (Color online) Temperature dependence of the ESR linewidth. Upper panel: $\mathbf{H}||(X+Y)$. Circles: low-field (high-g) component, squares: high field (low-g) component. All data are measured on the samples from the same batch. Lower panel: $\mathbf{H}||Y$. Filled and open symbols correspond to the data measured on samples from different batches. Experimental data were collected in different experimental setups operating at different frequencies, vertical lines mark approximate temperature boundaries for different experiments, and microwave frequencies of each experiment are given. Typical error bar size is around symbol size. Curves on both panels show empirical fit equations (see text and Table I).

in the $\mathbf{H}||(X+Y)$ orientation does not demonstrate such a peak, which is probably related to the very low intensity of the appearing weaker subcomponent which cause fitting procedure to lock on the main spectral subcomponent. Finally, on cooling below 1 K the linewidth of both components in the $\mathbf{H}||(X+Y)$ orientation increases again.

V. DISCUSSION

A. Recovery of the g tensor

Observed angular dependencies of the g factor can be fitted assuming uniaxial g tensor. As was described in Sec. III, g tensor is the same for the given ladder and orientations of the g tensors in inequivalent ladders are bound by the second order axis. Hence, directions of the main axis can be expressed via polar angles as $\mathbf{n}_{g1,2} = (\pm \sin\Theta\cos\phi; \cos\Theta; \pm\sin\Theta\sin\phi)$, here we count polar angle Θ from the second order axis $Y||b$, different signs correspond to the different ladders.

Least squares fit of our data (see Fig. 2) yields g-tensor components $g_\parallel = 2.296 \pm 0.010$ and $g_\perp = 2.040 \pm 0.006$ and angles $\Theta = (34.8 \pm 1.5)^\circ$ and $\phi = (178 \pm 4)^\circ$. Fit quality can be improved by assuming a general form of the g tensor. However, this results only in minor planar anisotropy (with principal g-factor values of 2.038 ± 0.010 and 2.058 ± 0.010), which is on the edge of experimental error.

The main axis of the g tensor within accuracy of our experiment lies in the (XY) plane of the crystal. This seems to be accidental as there is no symmetry reason to choose this plane in the monoclinic crystal. Orientations of the g-tensor main axes $\mathbf{n}_{g1,2}$ with respect to the crystal structure are shown in Fig. 1. We cannot decipher which of the orientations correspond to different ladders.

Found values of the main g-tensor components coincide with the values found in earlier powder high-field ESR experiment [15]. The value of the g factor for the $\mathbf{H}||a$ case $g_a = 2.17$ was found in Ref. [11] by magnetization fit, this value disagrees by 2% with the value $g_a^{(\mathrm{ESR})} = 2.130 \pm 0.005$ found in our experiment.

B. Interladder coupling estimation

Anisotropy of the g tensor opens a direct way to the estimation of interladder coupling. If the coupling between the ladders with different g-tensor orientation would be strong enough, then a common spin precession mode would be observed, a well known exchange narrowing phenomenon [16,17].

Instead, we observe well resolved ESR absorption signals from the inequivalent ladders. Thus, an upper limit on the interladder coupling can be estimated from the minimal splitting ΔH observed, which is around 40 Oe at the 17 GHz experiment (corresponds to components g-factor difference $\Delta g = 0.015$ in Fig. 2).

As it is known from the exchange narrowing theory, equally intense components with splitting $\Delta\omega$ will form a common precession mode if the coupling strength is above $J_c \simeq \hbar\Delta\omega$. Hence, we obtain an estimate $J_{\mathrm{inter}} < h\nu\frac{\Delta H}{H_{\mathrm{res}}} \simeq 5$ mK or about 0.5 μeV.

This value is in reasonable agreement with the earlier estimate of the interladder exchange coupling from the ordered

TABLE I. ESR linewidth: Empirical fit equations and parameters in different temperature ranges and at different orientations. For the orientations with two ESR components resolved (LF) and (HF) marks fit results for the low-field and high-field components correspondingly, (HF + LF) marks cases where linewidths of both components are close and their temperature dependencies are fitted jointly.

Temperature range and fit equations	Parameters	Typical fit accuracy	$\mathbf{H}\|\|Y$	$\mathbf{H}\|\|(X+Y)$	$\mathbf{H}\|\|(Y+Z)$
$T > 80$ K	ΔH_0, Oe	±5 Oe	46	45 (HF); 56 (LF)	
$\Delta H = \Delta H_0 + A\exp(-E_a/T)$	A, $\times 10^4$ Oe	±50%	5.9	1.7 (HF); 1.8 (LF)	
	E_a, K	±150 K	1510	1240 (HF); 1310 (LF)	
$15 < T < 80$ K	ΔH_∞, Oe	±5 Oe	35	35 (HF); 44(LF)	40 (HF+LF)
$\Delta H = \Delta H_\infty(1 + \Theta/T)$	Θ, K	±3 K	24	16 (HF); 22(LF)	14 (HF+LF)
$1.5 < T < 7$ K	$\Delta H_0'$, Oe	±2 Oe	10	15 (HF);15 (LF)	15(HF+LF)
$\Delta H = \Delta H_0' + A'\exp(-E_a'/T)$	A', $\times 10^2$ Oe	±30%	6.4	1.7 (HF);3.9 (LF)	5.3 (HF+LF)
	E_a', K	±1.5	14 (9.6[a])	6.4 (HF);8.4 (LF)	10.5(HF+LF)

[a]Value of $E_a' = 9.6$ K corresponds to the best fit with fixed parameter $\Delta H_0' = 0$ (see text).

phase boundary calculated in mean-field approximation [11] as $nJ'_{\mathrm{MF}} = 6.3$ μeV (here n is the number of coupled ladders, coupling considered to be equal in all directions). Note that our observation provides a direct estimate of the coupling between the unequivalently oriented ladders only.

C. Linewidth temperature dependence

Nonmonotonous temperature dependence of the linewidth indicates that spin precession relaxation is governed by different processes in the different parts of the studied temperature range. We fit this temperature dependence by a set of empirical equations as shown in Fig. 6 and discussed below. Values of the fit coefficients for the empiric equations used are gathered in Table I.

High temperature increase of the ESR linewidth (above 77 K) is naturally related to the spin-lattice relaxation: increase of the phonons population numbers leads to the increase of the relaxation rate. Linewidth dependencies can be fitted by the sum of the constant contribution describing the high-temperature spin-spin relaxation and an empirical activation law $\Delta H = \Delta H_0 + A\exp(-E_a/T)$. Activation energy is $E_a = (1400 \pm 150)$ K. Similar behavior with activation energy of the same order of magnitude was reported for other cuprates [18,19] and it was discussed [19] as a relaxation via excited state with a competing Jan-Teller distortion. However, detailed analysis of the lattice relaxation is beyond the scope of the present paper.

Lattice contribution vanishes with cooling. Shallow minimum of the linewidth at 70–100 K indicates that the phonon relaxation channel is practically frozen down here. Hence we assume that linewidth measured at 77 K is mostly due to spin-spin relaxation.

It is well known [20,21] that anisotropic spin-spin interactions are responsible for the spin-spin relaxation. Thus, ESR linewidth provides access to determine these interaction strengths. For the concentrated magnets the Dzyaloshinskii-Moriya interaction (which is allowed by the lattice symmetry of DIMPY) and symmetric anisotropic exchange interaction are the main contributions. Temperature dependence of the ESR linewidth is one of the physical effects to find which of theses anisotropic interactions dominates the linewidth.

Detailed description of the ESR linewidth in a quantum spin ladder is only emerging now: the case of spin ladder with symmetric anisotropic spin-spin coupling was considered recently by Furuya and Sato [22], a theory accounting for the uniform Dzyaloshinskii-Moriya interaction is still to be constructed. Theory of an ESR linewidth for a quantum $S = 1/2$ chain was developed by Oshikawa and Affleck more than decade ago [23]. We will apply their results to understand qualitatively temperature dependence of the ESR linewidth at high temperatures $T \gg J_{\mathrm{leg,rung}}$. Oshikawa and Affleck have demonstrated that contribution of the symmetric anisotropic exchange interaction to the ESR linewidth (exchange anisotropy in their terms) decreases with cooling. They also considered contribution of the staggered Dzyaloshinskii-Moriya interaction and have found that in this case ESR linewidth is increasing as $1/T^2$ at low temperatures. Oshikawa and Affleck demonstrated that at a high temperature limit staggered Dzyaloshinskii-Moriya interaction results in the linewidth increasing with cooling as $1/T$. As the high-temperature linewidth is determined by the pair spin correlations, this result should be actually the same for the staggered and uniform Dzyaloshinskii-Moriya interaction. This conclusion is in agreement with the results of Ref. [18] for the uniform Dzyaloshinskii-Moriya interaction in quasi-one-dimensional antiferromagnet Cs_2CuCl_4. Thus, increase of the linewidth with cooling below 80 K is a direct indication of the dominating role of the Dzyaloshinskii-Moriya interaction for the spin relaxation processes in DIMPY. To model first order of the $1/T$ expansion we fit our data by the law $\Delta H = \Delta H_\infty(1 + \Theta/T)$. Characteristic temperature Θ is anisotropic and varies from 15 to 25 K in the orientations presented in Fig. 6. This temperature scale is close to the exchange integral value in agreement with the results of Refs. [18,23].

The crude estimate of this interaction strength can be obtained from the linewidth at 80 K, which is approximately 50 Oe. As this temperature far exceeds the exchange integral scale high-temperature approximation can be used. We will discuss exact calculations below while describing angular dependence, but as an estimate one can write $\hbar\Delta\omega \sim \frac{D^2}{J}$ or $D \sim \sqrt{g\mu_B \Delta H J} \sim 0.3$ K.

As the temperature decreases below approximately 10 K linewidth starts to decrease. This decrease is naturally related

to the gapped spectrum of the spin ladder. At low temperatures magnetic properties of a spin ladder can be described by the triplet quasiparticles language and linewidth is then interpreted as an inverse lifetime of these quasiparticles, which is partially determined by their interaction. As temperature approaches scale of the energy gap, quasiparticle population numbers decreases, gas of the quasiparticles became diluted, and quasiparticle interaction contributions froze out. This results in the narrowing of the ESR absorption line with cooling. Microscopically this quasiparticle interaction could be related to anisotropic spin-spin couplings or to the possible magnon decays [24]. Detailed theoretical description of this regime awaits a separate effort, we performed a phenomenological thermoactivation fit of our data. The linewidth temperature dependence indeed follows thermoactivation law $\Delta H = \Delta H_0' + A' \exp(-E_a'/T)$ with activation energy $E_a' = 6.4$–14 K in different orientations. The largest activation energy is obtained for the field applied along the second order axis $\mathbf{H}||Y$. Most likely this result is an artifact due to the effects of field inhomogeneity in our experimental setup: the low temperature linewidth is minimal for $\mathbf{H}||Y$ and could be limited by experimental resolution. This leads to overestimation of a ΔH_0 parameter which in turn results in overestimation of the activation energy. Tentative fit of the $\mathbf{H}||Y$ data with a ΔH_0 value fixed to zero yield an activation energy of 9.6 K. Similar $\Delta H_0 = 0$ fits in other orientations lead to the smaller corrections of the determined activation energy.

The found activation energies lie in the interval between, approximately, $2\Delta(H)$ and $3\Delta(H)$, where $\Delta(H) \approx 3.0$ K is the gap at the experimental field of 17.5 GHz ESR experiment (see Fig. 5, right panel). This indicates that two- and/or three-particle interaction processes limit the quasiparticle lifetime in the low-temperature regime.

The peak of the linewidth around 1 K is related to the splitting of the ESR lines into subcomponents, its origin is related to the classical exchange narrowing phenomenon [16,17]. The exchange frequency became temperature dependent being related to the quasiparticles concentration. At low temperatures (low quasiparticles concentration) a split ESR line is observed, at higher temperatures (higher quasiparticles concentration) an effective exchange interaction between the quasiparticles gain efficiency and a common precession mode is formed. Crossover between these regimes results in the broadening of the ESR line. Similar effect is observed in other spin-gap magnets [25–27] and in other systems. [28]

Finally, definitive increase of the linewidth below 700 mK is observed for both ESR components at $\mathbf{H}||(X+Y)$ orientation. It is strongly anisotropic, the lowest temperature linewidth at $\mathbf{H}||(X+Y)$ orientation is three to four times larger than for the $\mathbf{H}||b$. Origin of this increase is unclear.

D. Angular dependence of the ESR linewidth

According to the theory of the exchange narrowed resonance spectra [29,30], the half-width at half-maximum for a single Lorentzian shaped line is given by

$$\Delta H = C\left[\frac{M_2^3}{M_4}\right]^{1/2}, \tag{2}$$

where C is a dimensionless constant of order unity, depending on how the wings of the Lorentzian profile drop at fields of the order of exchange field ($J/g\mu_B \gg \Delta H$) [30]; M_2 and M_4 are the second and fourth moments of resonance line, first introduced by Van Vleck [31],

$$M_2 = \frac{\langle[\mathcal{H}_{\text{anis}}, S^+][S^-, \mathcal{H}_{\text{anis}}]\rangle}{h^2\langle S^+S^-\rangle}, \tag{3}$$

$$M_4 = \frac{\langle[\mathcal{H}_{\text{ex}}, [\mathcal{H}_{\text{anis}}, S^+]][[S^-, \mathcal{H}_{\text{anis}}], \mathcal{H}_{\text{ex}}]\rangle}{h^4\langle S^+S^-\rangle}. \tag{4}$$

where $S^{\pm}$ denote left/right circular components of the total spin summed up over the whole sample, $\mathcal{H}_{ex}$ is the isotropic exchange Hamiltonian, and $\mathcal{H}_{\text{anis}}$ is the anisotropic one that does not commute with $\mathcal{H}_{\text{ex}}$, hence causing broadening of the resonance line.

Analysis of the ESR linewidth based on calculation of the spectral moments is a well developed method which allows us to identify the nature of spin-spin interactions and estimate their magnitudes in magnetically concentrated systems [32]. Its benefit is that in a high temperature limit ($T \to \infty$) an exact expression for linewidth can be found for an arbitrary spin system, whatever space dimension and exchange couplings [21,33].

In the present paper we apply the "method of moments" to a strong-leg spin ladder system, described by Hamiltonian (1) with uniform Dzyaloshinskii-Moriya interaction

$$\mathcal{H}_{\text{DM}} = \sum_i \sum_{l=1,2} \mathbf{D}_l[\mathbf{S}_{l,i} \times \mathbf{S}_{l,i+1}], \tag{5}$$

here i enumerates rungs of the ladder and l enumerates legs of the ladder, DM vectors on the legs are considered arbitrary for the moment ($\mathbf{D}_1 \neq \mathbf{D}_2$). Following Refs. [14,18] calculations of the second and fourth moments were performed in a laboratory coordinate system (xyz) with the z axis chosen along the externally applied magnetic field. Substituting Eq. (5) into Eqs. (3) and (4) and using the corresponding commutation relations for $S = 1/2$ spin operators, for the linewidth Eq. (2) in the high temperature limit we have

$$\Delta H_{\infty}^{\text{DM}}(\text{Oe}) = C \sum_{l=1,2} \frac{\left[D_x^2 + D_y^2 + 2D_z^2\right]_l}{4\sqrt{2}\mu_B \tilde{J}_D g(\theta,\phi)}, \tag{6}$$

where $\tilde{J}_D = \sqrt{J_{\text{leg}}^2 + 2J_{\text{rung}}^2}$ is an average exchange integral [33], and angular dependence is determined by the transformation of the DM vector from the crystallographic system into the laboratory coordinate system:

$$\begin{aligned} D_x &= D_X \cos\beta\cos\alpha + D_Y \cos\beta \sin\alpha - D_Z \sin\beta, \\ D_y &= D_Y \cos\alpha - D_X \sin\alpha, \\ D_z &= D_X \sin\beta\cos\alpha + D_Y \sin\beta\sin\alpha + D_Z \cos\beta. \end{aligned} \tag{7}$$

here $D_{X,Y,Z}$ are the components of the DM vector in the crystallographic Cartesian system, $D_{x,y,z}$ are the components of the DM vector in a laboratory coordinates, angles α and β define orientation of the laboratory coordinate system (xyz), where the Zeeman term in Eq. (1) takes the diagonal form $g\mu_B H S^z$ with

$$g = \sqrt{A^2 + B^2 + C^2}, \tag{8}$$

where

$$A = g_{XX}\sin\widetilde{\Theta}\cos\widetilde{\phi} + g_{XY}\cos\widetilde{\Theta} + g_{XZ}\sin\widetilde{\Theta}\sin\widetilde{\phi},$$
$$B = g_{YX}\sin\widetilde{\Theta}\cos\widetilde{\phi} + g_{YY}\cos\widetilde{\Theta} + g_{YZ}\sin\widetilde{\Theta}\sin\widetilde{\phi},$$
$$C = g_{ZX}\sin\widetilde{\Theta}\cos\widetilde{\phi} + g_{ZY}\cos\widetilde{\Theta} + g_{ZZ}\sin\widetilde{\Theta}\sin\widetilde{\phi},$$

and

$$\cos\alpha = \frac{A}{\sqrt{A^2+B^2}}, \quad \cos\beta = \frac{C}{\sqrt{A^2+B^2+C^2}},$$

here polar $\widetilde{\Theta}$ and azimuthal $\widetilde{\phi}$ angles define the direction of external magnetic field, so that $\widetilde{\Theta}$ and $\widetilde{\phi}$ are counted from Y and X axes, respectively, as during the g-tensor recovery procedure.

Note that by setting $J_{\rm rung} = 0$ and $\mathbf{D}_1 = \mathbf{D}_2$ in Eq. (6) we immediately arrive to the known result for the 1D Heisenberg chain with uniform DM interaction (see formula (16) in Ref. [18]).

DIMPY has two inequivalent ladders with different g tensors and DM vectors. In accordance with crystal symmetry of the DIMPY (see Sec. III), the legs within the same ladder are linked by inversion, so that

$$\hat{\mathbf{g}}_1^{(k)} = \hat{\mathbf{g}}_2^{(k)}, \quad \mathbf{D}_1^{(k)} = -\mathbf{D}_2^{(k)} \quad (k = 1 \text{ or } 2), \tag{9}$$

here the upper index ($k = 1,2$) denotes the inequivalent ladders and the lower index enumerates legs of the ladder. The legs of inequivalent ladders are linked by screw rotation along the second order axis, hence

$$\begin{aligned} \mathbf{D}_l^{(2)} &= C_2(Y)\mathbf{D}_l^{(1)}, \\ \hat{\mathbf{g}}_l^{(2)} &= C_2(Y)\hat{\mathbf{g}}_l^{(1)}C_2(Y)^{-1} \quad (l = 1,2). \end{aligned} \tag{10}$$

Having known directions of the main axes of g tensors (see Sec. V A), it is easy to find their components referred to crystallographic coordinates for nonequivalent spin ladders

$$\hat{g}^{(1,2)} = \begin{pmatrix} 2.128 & \mp 0.12 & -0.008 \\ \mp 0.12 & 2.214 & \pm 0.005 \\ -0.008 & \pm 0.005 & 2.038 \end{pmatrix}, \tag{11}$$

where upper (down) sign corresponds to the ladder with upper (down) sign of $\mathbf{n}_g$.

Simulation of experimental data on the linewidth angular dependence by Eq. (6) showed that the Dzyaloshinskii-Moriya interaction describes the angular variation of the linewidth in DIMPY well enough (within experimental error). However, a model including Dzyaloshinskii-Moriya interaction only predicts a value of linewidth which is systematically less than the experimental values by about 12 Oe. This fact indicates that there is an additional (small compared to DM interaction) source of the line broadening in DIMPY. The modeled values of the linewidth can be reconciled with the experimental ones by adding isotropic contribution $\Delta H_0 = 12$ Oe, which can be probably ascribed to the residual spin-lattice relaxation, or by considering other anisotropic spin-spin couplings. Contribution to the linewidth from dipole-dipole interaction is quite small for DIMPY and at the shortest distance between Cu ions ($r = a \approx 7.5$ Å) following conventional estimation [34] it does not exceed ~0.5 Oe. Additional broadening in DIMPY can be related to SAE interaction along legs and rungs of the spin ladders which usually appear as further sources of ESR line broadening beyond the dominant DM interaction [18,35]. The contribution to the linewidth due to SAE interaction is derived in Appendix A.

We do not consider effects of spin diffusion [36,37] known to be of importance in some of the low-dimensional magnets since within accuracy of our experiment we do not observe any deviations from a Lorentzian line shape of the ESR absorption, such deviation being one of the key prediction of the spin diffusion theory.

Taking into account symmetry relations [Eqs. (9), (10), (11), and (A3)] and, for definiteness setting $\mathbf{D}_1^{(1)} = \mathbf{D}$, $\hat{\mathbf{A}}_1^{(1)} = \hat{\mathbf{A}}$, the fitting of linewidth angular dependence yields $D_X = 0.21$, $D_Y = -0.20$, $D_Z = 0.11$ K and almost diagonal exchange tensor with components $J_{XX} = 0.11$, $J_{YY} = -0.04$, $J_{ZZ} = -0.07$, $J_{XY} = -0.021$ K, and $J_{XZ} = J_{YZ} = 0$. During simulation the Lorentzian profile with exponential wings was assumed, which implies $C = \pi\sqrt{2}$. Note that fit for DM vector components essentially locks at extreme values of the linewidth and thus is reliable with approximately 10% accuracy. Fit for the SAE tensor components, on the contrary, depends upon weaker deviations of the model curve from the experimental data, contribution of the SAE coupling, and especially its anisotropy is close to experimental error (see Fig. 2). Thus, with the accuracy of the present experiment SAE fit results can be considered as an estimate only.

Directions of the found $\mathbf{D}$ vectors are shown in Fig. 1. Components of the DM vector and SAE tensor given above correspond to the ladder with the g-tensor main axis orientation $\mathbf{n}_{g1} = (\sin\Theta\cos\phi; \cos\Theta; \sin\Theta\sin\phi) \approx (-0.57; 0.82; 0)$ (when comparing with Fig. 1 note that $\mathbf{n}_g$ and $-\mathbf{n}_g$ are physically equivalent), angle between $\mathbf{D}$ and $\mathbf{n}_g$ vectors [reduced to $(-\frac{\pi}{2}; \frac{\pi}{2})$ range for convenience] is approximately 23°. Magnitude of the obtained Dzyaloshinskii-Moriya vector $|\mathbf{D}| = 0.31$ K agrees well with the crude estimation above (Sec. V C).

As it is seen from Fig. 2, taking into consideration only an exchange mechanisms of spin anisotropy within the legs of ladders gives a good compliance with experiment. However, it is necessary to stress out, that without DM interaction SAE coupling only (see Appendix A) totally failed to give a correct description of the angular dependence of linewidth in DIMPY.

Our simulation shows that absolute value as well as angular anisotropy of the linewidth are predominantly determined by the DM interaction, while contribution to the linewidth due to SAE interaction is relatively small. Similar behavior of ESR linewidth with coexistent contributions from DM and SAE interactions within $S = 1/2$ antiferromagnetic chains was observed in high symmetry crystal structure $KCuF_3$ [35].

The found DM vector has not only transverse but also a nonzero *longitudinal* (with respect to the Cu-Cu exchange bond) component within the legs. Such a result does not contradict with the general rules for DM vector, established by Moriya [38] based on the general symmetry grounds for a pair of exchange interacting ions. Moreover, a simple analysis of the recovered g tensors (see Sec. V A) leads to the same conclusion about the direction of the DM vector. Since the axial component of the g tensor has a maximal

value, then the ground state orbitals of Cu^{2+} ions (typically "$\tilde{x}^2 - \tilde{y}^2$"-like symmetry and $\tilde{z}||\mathbf{n}_g$) should predominantly lie within the plane perpendicular to the main axis of a g tensor, because the maximal matrix element ($\langle\tilde{x}^2 - \tilde{y}^2|l_g|\tilde{x}\tilde{y}\rangle = -2\imath$) relevant to spin-orbital coupling appears only in the case when an external magnetic field is applied parallel to the main axis of the g tensor. For the same reason an effective DM vector predominantly should lie along the main axis of the g tensor. It should be noted that a conventional rule determining DM vector as $\mathbf{D} \propto [n_1 \times n_2]$ [39,40], where n_1 and n_2 are unit vectors connecting an exchange interacting ions with a bridging ion, is not applicable in the present case. Possible failure of this rule was mentioned before in Ref. [41], referring to the features of exchange process through two bridging ions, which is also the case of DIMPY (see Fig. 1).

Thus, analysis of the ESR linewidth allowed us to conclude that the DIMPY is a rare case of compound in which the DM vector has a component along the line connecting the pair of exchange interacting ions. This is a consequence of low crystal symmetry of DIMPY and nontrivial orbital ordering.

E. Low-temperature subcomponents appearance

First, we recall main observations on the subcomponent appearance. ESR components split around 1 K into two subcomponents, one of which is much weaker. The splitting is best observed at $\mathbf{H}||(X + Y)$ orientation. Position of the weaker subcomponent with respect to the stronger subcomponent is different for both ESR absorption components. Maximal splitting is about 150 Oe and it decreases as the resonance field approaches critical field, the weaker subcomponent became unresolvable at the fields above 2/3 of the critical field. Activation energies for the stronger and weaker subcomponents are different.

All these observations can be explained as an effect of the zero-field splitting of triplet sublevels. This effect was already observed for various spin-gap magnets, e.g., $TlCuCl_3$ [25] or PHCC [26]. Anisotropic interactions lift degeneracy of the $S = 1$ triplet state and frequencies of the dipolar transitions $|S^z = +1\rangle \leftrightarrow |S^z = 0\rangle$ and $|S^z = -1\rangle \leftrightarrow |S^z = 0\rangle$ become different. Here we assume, which is perfectly valid for the case of DIMPY, that the anisotropy is very small and spin projection on the field direction S^z can be considered as a good quantum number. Therefore, in the presence of such an anisotropy the resonance fields for $|S^z = +1\rangle \leftrightarrow |S^z = 0\rangle$ and $|S^z = -1\rangle \leftrightarrow |S^z = 0\rangle$ transitions in the constant frequency ESR experiment would differ and ESR absorption split into two subcomponents.

Observed difference of the activation energies for the absorption subcomponents and dependence of the activation energy on the microwave frequency used in the experiment is a direct consequence of this explanation. The ESR intensity at low temperature is determined by the population of the lowest sublevel. Hence, for the $|S^z = +1\rangle \leftrightarrow |S^z = 0\rangle$ transition, the activation energy is $\Delta \approx \Delta_0 - g\mu_B H_{\rm res} = \Delta_0 - h\nu$, being determined by the population of the $|S^z = +1\rangle$ sublevel (energy of this sublevel decreases with field, see inset in Fig. 5). In the same time the activation energy for the $|S^z = -1\rangle \leftrightarrow |S^z = 0\rangle$ remains constant (and equal to Δ_0), since the energy of $|S^z = 0\rangle$ sublevel is field independent. The dependencies of the activation energy on the microwave frequency of the ESR experiment are described by this model parameter-free using the zero-field gap value of 0.33 meV from the inelastic neutron scattering experiment [9,10].

Behavior of the sublevels of the spin-gap magnet in the vicinity of the critical field is a long-discussed problem. There is a general macroscopic (or bosonic) approach of Refs. [3,5] and a 1D fermionic approach of Tsvelik [4] developed for the spin chains. A fermionic model of Tsvelik yields results formally equivalent to the results of perturbation treatment of anisotropic interactions [42]. Thus, within the fermionic approach, the sublevels behave linearly in the vicinity of the critical field and the splitting of the ESR subcomponent should be then field independent. The bosonic model, on the contrary, predicts a square-root-like approach to the critical field for the low-energy sublevel, while field dependence of the high-energy sublevel remains linear in the vicinity of the critical field. Therefore, subcomponents splitting will change close to the critical field. However, this nonlinearity of the bosonic model extends only in the small vicinity of the critical field $(H_c - H) \sim \Delta E/\mu_B \sim \Delta H$, here ΔE is the zero-field triplet sublevels splitting and $\Delta H \simeq 150$ Oe is the observed subcomponents splitting. We observe (Fig. 4) that the observed splitting is halved (compare 50.18 and 26.30 GHz curves in Fig. 4) in the field of about 2/3 of the critical field ($H_c \simeq 30$ kOe, zero-field gap of 0.33 meV corresponds to the frequency of 80 GHz), i.e., well below this nonlinearity range. This probably indicates that field evolution of the split subcomponents follows some other laws on approaching the critical field. Similar behavior of the ESR line split by the uniform Dzyaloshinskii-Moriya interaction was recently reported for a quasi-1D antiferromagnet Cs_2CuCl_4 [43].

Under an assumption that the uniform Dzyaloshinskii-Moriya interaction along the legs of the ladder is responsible for the observed splitting, the anisotropy axis has to be aligned along the **D** vector. We calculated effects of the DM coupling perturbatively for the limiting case of the strong-rung ladder (see Appendix B). Interdimer DM interaction mixes one- and two-particle excited $S^z = \pm 1$ states which results in the triplet sublevels splitting by $\delta E = \frac{D^2}{2J}$, $S^z = \pm 1$ sublevels being shifted down. This corresponds to the easy-axis anisotropy for the triplet excitations, **D** direction being the easy-axis direction. Taking the magnitude of the DM vector $D \approx 0.31$ K as estimated from the high-temperature ESR linewidth analysis and substituting an energy gap of 0.33 meV as an exchange parameter of the perturbative model we obtain an estimate of the sublevels splitting $\delta E \simeq 10$ mK which corresponds to maximal subcomponents splitting of about 80 Oe, factor of 2 less than the experimentally observed value. However, perturbative treatment starting from the uninteracting dimers is at best a qualitative model for a strong-leg ladder and a detailed description of a strong-leg spin ladder with uniform Dzyaloshinskii-Moriya interaction needs a separate theoretical effort.

We cannot unambiguously determine the type of the anisotropy from our experimental observation since our setup does not allow us to take an angular dependence at the He-3 temperature range. However, as it is known from the formally similar problem of the $S = 1$ ion in a crystal field [20,21], the effective anisotropy constant changes monotonously with field

rotating away from the anisotropy axis $C_{\rm eff} = \frac{C}{2}(3\cos^2\xi - 1)$, where ξ is an angle counted from the anisotropy axis z and anisotropy C enters spin Hamiltonian as $C(S^z)^2$. It is maximal at the field parallel to the anisotropy axis, it changes sign and decreases by the factor of 2 at the orthogonal orientation of the magnetic field, and it turns to zero at a magic angle. Thus, as the splitting observed for the high-field component is larger than that for the low-field component (approximately 150 vs 110 Oe, see Fig. 4) and weaker subcomponents are located on different sides from the main subcomponents, we find it more likely that the high-field component corresponds to the ladder with the magnetic field close to the true anisotropy axis. In this case, as for the field applied close to the anisotropy axis, the weaker subcomponent is located to the right from the stronger subcomponent, the splitting of the triplet sublevels follows the easy-axis type of anisotropy, the energy of $S^z = \pm 1$ states being lower than energy of the $S^z = 0$ state in zero field. Zero-field splitting of triplet sublevels can be estimated as 20 mK (which would result in the maximal splitting of ESR subcomponents by 150 Oe).

However, this tentative identification of the anisotropy axis deviates from the simple model of DM interaction only: as the vectors $\mathbf{D}$ and $\mathbf{n}_g$ are quite close for the given ladder the low-field component (corresponding to the higher longitudinal g factor) should then be closer to the anisotropy axis. A possible reason for this deviation is the effect of symmetric anisotropic exchange on the rungs of the ladder (see Appendix B). SAE coupling on the rungs of the ladder is of particular importance here: being smaller in magnitude than the DM coupling constant and smaller than the SAE coupling along the legs of the ladder, SAE coupling on the rungs of the ladder enters to the triplet sublevels splitting linearly, while contributions of DM coupling and SAE coupling along the leg of the ladder are quadratic. This is contrary to the linewidth calculations where all couplings enter quadratically. Zero-field splitting of triplet sublevels by 20 mK corresponds within a simple one-dimer model (see Appendix B) to the SAE coupling constant $A_{\rm rung} = -40$ mK [value of -40 mK corresponds to the notations of Hamiltonian (B6) it recalculates to the tensor with diagonal values {13 mK; 13 mK; -26 mK} in a zero-trace calibration of SAE used in linewidth analysis]. This estimate is close to the magnitude of SAE coupling parameters estimated from the high-temperature linewidth, however linewidth analysis cannot discern between SAE couplings along the leg and along the rung of the ladder. The anisotropic part of the dipolar interaction on the rungs of the ladder has formally the same form as SAE coupling but, due to the large interatomic distance on the rung (8.9 Å), characteristic dipolar energy $\frac{\mu_B^2}{d^3} \simeq 0.9$ mK is too small to be of effect.

Thus, description of the subcomponents splitting in DIMPY lies beyond the simple model with DM interaction only, the observed splitting is a result of interplay between DM and SAE couplings.

VI. CONCLUSIONS

The strong-leg spin ladder system DIMPY is an established test example of the Heisenberg spin ladder. However, anisotropic spin-spin interactions, and in particular Dzyaloshinskii-Moriya interaction of intriguing geometry (uniform along the leg of the ladder and exactly opposite on the other leg), give rise to a family of interesting phenomena.

We have estimated parameters of Dzyaloshinskii-Moriya interaction from high-temperature data. We observe splitting of the ESR line at low temperatures which is related to the zero-field splitting of the triplet sublevels caused by the interplay of Dzyaloshinskii-Moriya interaction and symmetric anisotropic exchange coupling. Finally, we observe series of crossovers between different regimes of relaxation of spin precession on cooling from room temperature to 400 mK.

We present qualitative explanations of our observations. Simple geometry of the exchange couplings and anisotropic spin-spin interactions makes DIMPY one of the few candidates for the model-free microscopic description of the effects of anisotropic interactions on the properties of a spin-gap magnet, which is still awaiting for a theoretical effort.

ACKNOWLEDGMENTS

We thank Dr. A. B. Drovosekov (P. L. Kapitza Institute) for the assistance with ESR experiment above 77 K and Professor A. K. Vorobiev (M. V. Lomonosov Moscow State University) for the possibility to perform reference measurements with the X-band spectrometer. We thank Dr. K. Povarov, Professor M. V. Eremin, and Professor A. I. Smirnov for valuable and stimulating discussions. Authors acknowledge usage of "Balls & Sticks" software to build crystal structure images. The work was supported by Russian Foundation for Basic Research Grant No. 15-02-05918 and Russian Presidential Grant for the Support of the Leading Scientific Schools No. 5517.2014.2. M.F. work was supported by the Russian Government Program of Competitive Growth of Kazan Federal University. This work was partially supported by the Swiss National Science Foundation, Division 2.

APPENDIX A: LINEWIDTH CONTRIBUTION BY A SAE INTERACTION ALONG THE LEGS

Symmetric anisotropic exchange (SAE) coupling is allowed both on the rungs and on the legs of the ladder. Our aim here is to demonstrate that SAE coupling can explain contribution of about 20% of the total linewidth that cannot be described by DM coupling alone. We will focus here on a SAE coupling along the legs of the ladder. We have checked that a SAE coupling along the rung yields similar angular dependence and its contribution differs only by some numerical scaling factor. However, we expect that contribution of the SAE couplings on the rungs should be small in a strong-leg ladder since the overlapping of the orbitals along the rung is smaller.

An expression for ESR linewidth due to a SAE coupling along the legs of spin ladder is derived similarly as was done for a DM one in Sec. V D, applying

$$\mathcal{H}_{\rm SAE} = \sum_i \sum_{l=1,2} \mathbf{S}_{l,i} \hat{\mathbf{A}}_l \mathbf{S}_{l,i+1} \tag{A1}$$

to Eqs. (3), (4), and (2) in the framework of "method of moments," that in the high temperature limit of $S = 1/2$

leads to

$$\Delta H_{\infty}^{\mathrm{SAE}} = C \sum_{l=1,2} \frac{\left[(2\lambda_{zz} - \lambda_{xx} - \lambda_{yy})^2 + 10\left(\lambda_{xz}^2 + \lambda_{yz}^2\right) + (\lambda_{xx} - \lambda_{yy})^2 + 4\lambda_{xy}^2\right]_l}{8\sqrt{6}\mu_B \tilde{J}_S g(\theta,\phi)}, \tag{A2}$$

where $\tilde{J}_S = \sqrt{J_{\mathrm{leg}}^2 + 2/3 J_{\mathrm{rung}}^2}$, and the exchange-tensor components in the laboratory coordinates $\lambda_{\eta\gamma}(\alpha,\beta)$ $(\eta,\gamma = x,y,z)$ are defined by transformation given in Ref. [14] [see formulas (A2)–(A4) therein] and, as usually, are expressed via the intrinsic exchange parameters $J_{\mu\tau}$ of symmetric tensor $\hat{\mathbf{A}}$ in crystallographic coordinates $(\mu,\tau = X,Y,Z)$.

In accordance with crystal symmetry of the DIMPY (see Sec. III), symmetric exchange tensors on the legs of the same ladder are equal, while on the legs of inequivalent ladders they are related by a screw rotation along the second order axis, that is

$$\begin{aligned} &\hat{\mathbf{A}}_1^{(k)} = \hat{\mathbf{A}}_2^{(k)} \quad (k = 1 \text{ or } 2), \\ &\hat{\mathbf{A}}_l^{(2)} = C_2(Y)\hat{\mathbf{A}}_l^{(1)}C_2(Y)^{-1} \quad (l = 1,2). \end{aligned} \tag{A3}$$

Generally, taking into account the relation of $J_{\eta\gamma} = J_{\gamma\eta}$ for a symmetric tensor, an exchange tensor has six different components, constrained by $\mathrm{Tr}J_{\eta\gamma} = 0$ condition. However, since the anisotropy of the g tensor and the tensor of SAE coupling originates from the same spin-orbital interactions, accidental smallness of g_{XZ} and g_{YZ} components allows us to assume $J_{XZ} = J_{YZ} = 0$ during the fitting procedure. We have found that the remaining four components of the SAE tensor are enough to reproduce our data.

APPENDIX B: PERTURBATIVE TREATMENT OF TRIPLET SUBLEVELS SPLITTING BY UNIFORM DM AND SAE COUPLINGS

Strong-rung $J_{\mathrm{rung}} \gg J_{\mathrm{leg}}$ limit allows us to use wave functions of the isolated dimers as a zero-order approximation. For the dimer located at the nth rung wave function of the ground state is $\psi_{n0} = \frac{1}{\sqrt{2}}(|\uparrow\downarrow\rangle_n - |\downarrow\uparrow\rangle_n)$ and wave functions of the excited triplet are $\psi_{n11} = |\uparrow\uparrow\rangle_n$, $\psi_{n10} = \frac{1}{\sqrt{2}}(|\uparrow\downarrow\rangle_n + |\downarrow\uparrow\rangle_n)$, and $\psi_{n1-1} = |\downarrow\downarrow\rangle_n$. Wave function of the collective ground state is $\Psi^{(0)} = \prod_p \psi_0^{(p)}$ and single-particle excited states with the excitation at the nth dimer can be built as

$$\Psi_{n11}^{(1)} = \prod_{p=0}^{n-1} \psi_{p0}\psi_{n11} \prod_{p=n+1}^{N} \psi_{p0} \tag{B1}$$

and similarly for other spin projections. Many particle excited state can be constructed similarly keeping in mind hard-core repulsion as only one excited state per dimer is allowed.

One-particle states are N-fold degenerated, this degeneration will be lifted by interdimer exchange coupling J_{leg} giving rise to excitations dispersion.

We consider the effect of interdimer DM interaction (5) with DM vectors oppositely aligned on the legs of the ladder. This configuration conserves symmetry axis (direction of the DM vector, which we will use as z direction), thus excitations will have well defined S^z values. Interdimer DM interaction can then be expressed as

$$\begin{aligned} V = \frac{D}{2\imath} \sum_n [&S_{1,n}^- S_{1,n+1}^+ - S_{1,n}^+ S_{1,n+1}^- \\ &- S_{2,n}^- S_{2,n+1}^+ + S_{2,n}^+ S_{2,n+1}^-]. \end{aligned} \tag{B2}$$

By applying this operator to the ground state and to one-particle excited states we obtain

$$V\Psi^{(0)} = 0, \tag{B3}$$

$$V\Psi_{n10}^{(1)} = 0, \tag{B4}$$

$$V\Psi_{n11}^{(1)} = \frac{D}{2\imath}\left(-\Psi_{n10;(n+1)11}^{(2)} + \Psi_{n10;(n-1)11}^{(2)}\right), \tag{B5}$$

here $\Psi_{n10;m11}^{(2)}$ are two-particle excited states with $S = 1, S^z = 0$ excitation on the nth rung and $S = 1, S^z = 1$ excitation on the mth rung.

Thus, interdimer DM interaction mixes $S^z = \pm 1$ single-particle excited states with $S^z = \pm 1$ two-particle excited states. This mixing results in the second order perturbative correction to the energy of the single-particle state $\delta E = -\frac{D^2}{2J_{\mathrm{rung}}}$, $S^z = \pm 1$ being shifted down. As this correction is the same for all $S^z = \pm 1$ states, weak interdimer Heisenberg coupling J_{leg} will not affect it.

This result differs from the effect of intradimer DM interaction which mixes $S = 1, S^z = 0$ state with $S = 0$ state and shifts the energy of the $S = 1, S^z = 0$ up by $\frac{D^2}{4J_{\mathrm{rung}}}$. However, both interdimer and intradimer DM interaction results in the easy-axis anisotropy for the triplet excitations (energy of the $S^z = \pm 1$ states is lower than the energy of the $S^z = 0$ state).

Note also that the effective anisotropy for the triplet excitations is easy axis, while usual anisotropy due to DM interaction (e.g., anisotropy of the order parameter in the ordered state of an antiferromagnet) is of easy plane type. This "inversion" of anisotropy seems to be a common feature of all spin-gap magnets: it was obtained by perturbative analysis of the role of single-ion anisotropy in a Haldane magnet [44] and was observed in a Haldane magnet $PbNi_2V_2O_8$ [45], similar inversion of the anisotropy type between the anisotropy of triplet excitations and order parameter anisotropy in a field-induced ordered phase of a spin-gap magnet follows from macroscopic approach [5].

Effect of the symmetric anisotropic coupling on a strong-rung ladder can be considered similarly. Our aim here is to illustrate that its contribution is linear on a coupling parameter along the rung so we consider simple axial SAE coupling in the form

$$V = A_{\mathrm{leg}} \sum_{n,j} S_{j,n}^z S_{j,n+1}^z + A_{\mathrm{rung}} \sum_n S_{1,n}^z S_{2,n}^z, \tag{B6}$$

here n enumerates rungs (dimers) and j enumerates legs of the ladder (spins in the dimer), A_{leg} and A_{rung} are

SAE coupling constants along the leg and rung of the ladder.

By applying this operator to the ground state and to the one-particle excited states one can ascertain that SAE coupling along the legs mixes ground sate and single-particle states with two-particle states and will give some corrections in the second order of perturbations, while SAE coupling on the rungs gives energy corrections already in the first order on the coupling parameter: energies of the ground state and of the $S^z = 0$ component of triplet state are shifted (per dimer) by $-\frac{1}{4}A_{\text{rung}}$, while energies of the $S^z = \pm 1$ components are shifted by $+\frac{1}{4}A_{\text{rung}}$. Zero-field splitting of triplet levels equal to $\frac{1}{2}A_{\text{rung}}$ appears, its type (easy axis or easy plane) depends on the sign of coupling parameter A_{rung}, which can be both positive and negative.

[1] H. J. Mikeska and A. K. Kolezhuk, Lect. Notes Phys. **645**, 1 (2004).
[2] M. Hagiwara, L. P. Regnault, A. Zheludev, A. Stunault, N. Metoki, T. Suzuki, S. Suga, K. Kakurai, Y. Koike, P. Vorderwisch, and J.-H. Chung, Phys. Rev. Lett. **94**, 177202 (2005).
[3] I. Affleck, Phys. Rev. B **46**, 9002 (1992).
[4] A. M. Tsvelik, Phys. Rev. B **42**, 10499 (1990).
[5] A. M. Farutin and V. I. Marchenko, Zh. Eksp. Teor. Fiz. **131**, 860 (2007) [JETP **104**, 751 (2007)].
[6] A. K. Kolezhuk, V. N. Glazkov, H. Tanaka, and A. Oosawa, Phys. Rev. B **70**, 020403 (2004).
[7] K. Yu. Povarov, A. I. Smirnov, O. A. Starykh, S. V. Petrov, and A. Ya. Shapiro, Phys. Rev. Lett. **107**, 037204 (2011).
[8] A. Shapiro, C. P. Landee, M. M. Turnbull, J. Jornet, M. Deumal, J. J. Novoa, M. A. Robb, and W. Lewis, J. Am. Chem. Soc. **129**, 952 (2007).
[9] T. Hong, Y. H. Kim, C. Hotta, Y. Takano, G. Tremelling, M. M. Turnbull, C. P. Landee, H.-J. Kang, N. B. Christensen, K. Lefmann, K. P. Schmidt, G. S. Uhrig, and C. Broholm, Phys. Rev. Lett. **105**, 137207 (2010).
[10] D. Schmidiger, S. Mühlbauer, S. N. Gvasaliya, T. Yankova, and A. Zheludev, Phys. Rev. B **84**, 144421 (2011).
[11] D. Schmidiger, P. Bouillot, S. Mühlbauer, S. Gvasaliya, C. Kollath, T. Giamarchi, and A. Zheludev, Phys. Rev. Lett. **108**, 167201 (2012).
[12] J. L. White, C. Lee, Ö. Günaydin-Şen, L. C. Tung, H. M. Christen, Y. J. Wang, M. M. Turnbull, C. P. Landee, R. D. McDonald, S. A. Crooker, J. Singleton, M.-H. Whangbo, and J. L. Musfeldt, Phys. Rev. B **81**, 052407 (2010).
[13] M. Ozerov, M. Maksymenko, J. Wosnitza, A. Honecker, C. P. Landee, M. M. Turnbull, S. C. Furuya, T. Giamarchi, and S. A. Zvyagin, arXiv:1509.02056.
[14] R. M. Eremina, M. V. Eremin, V. N. Glazkov, H.-A. K. von Nidda, and A. Loidl, Phys. Rev. B **68**, 014417 (2003).
[15] H. Ohta, T. Yamasaki, S. Okubo, T. Sakurai, M. Fujisawa, and H. Kikuchi, J. Phys.: Conf. Ser. **320**, 012026 (2011).
[16] P. W. Anderson, J. Phys. Soc. Jpn. **9**, 316 (1954).
[17] L. H. Piette and W. A. Anderson, J. Chem. Phys. **30**, 899 (1959).
[18] M. A. Fayzullin, R. M. Eremina, M. V. Eremin, A. Dittl, N. van Well, F. Ritter, W. Assmus, J. Deisenhofer, H.-A. K. von Nidda, and A. Loidl, Phys. Rev. B **88**, 174421 (2013).
[19] M. Heinrich, H.-A. Krug von Nidda, A. Krimmel, A. Loidl, R. M. Eremina, A. D. Ineev, B. I. Kochelaev, A. V. Prokofiev, and W. Assmus, Phys. Rev. B **67**, 224418 (2003).
[20] A. Abragam and B. Bleaney, *Electron Paramagnetic Resonance of Transition Ions* (Clarendon, Oxford, 1970).
[21] S. Al'tshuler and B. Kozyrev, *Electron Paramagnetic Resonance* (Academic, New York, 1964).
[22] S. C. Furuya and M. Sato, J. Phys. Soc. Jpn. **84**, 033704 (2015).
[23] M. Oshikawa and I. Affleck, Phys. Rev. B **65**, 134410 (2002).
[24] M. E. Zhitomirskii and A. L. Chernyshev, Rev. Mod. Phys. **85**, 219 (2013).
[25] V. N. Glazkov, A. I. Smirnov, H. Tanaka, and A. Oosawa, Phys. Rev. B **69**, 184410 (2004).
[26] V. N. Glazkov, T. S. Yankova, J. Sichelschmidt, D. Hüvonen, and A. Zheludev, Phys. Rev. B **85**, 054415 (2012).
[27] S. A. Zvyagin, J. Wosnitza, J. Krzystek, R. Stern, M. Jaime, Y. Sasago, and K. Uchinokura, Phys. Rev. B **73**, 094446 (2006).
[28] D. B. Chestnut and W. D. Phillips, J. Chem. Phys. **35**, 1002 (1961).
[29] P. W. Anderson and P. R. Weiss, Rev. Mod. Phys. **25**, 269 (1953).
[30] T. G. Castner, Jr. and M. S. Seehra, Phys. Rev. B **4**, 38 (1971).
[31] J. H. Van Vleck, Phys. Rev. **74**, 1168 (1948).
[32] D. V. Zakharov *et al.*, in *Quantum Magnetism*, edited by B. Barbara *et al.* (Springer, Dordrecht, 2008).
[33] D. L. Huber, G. Alejandro, A. Caneiro, M. T. Causa, F. Prado, M. Tovar, and S. B. Oseroff, Phys. Rev. B **60**, 12155 (1999).
[34] I. Yamada, M. Nishi, and J. Akimutsu, J. Phys.: Condens. Matter **8**, 2625 (1996).
[35] M. V. Eremin, D. V. Zakharov, H.-A. K. von Nidda, R. M. Eremina, A. Shuvaev, A. Pimenov, P. Ghigna, J. Deisenhofer, and A. Loidl, Phys. Rev. Lett. **101**, 147601 (2008).
[36] R. E. Dietz, F. R. Merritt, R. Dingle, D. Hone, B. G. Silbernagel, and P. M. Richards, Phys. Rev. Lett. **26**, 1186 (1971).
[37] R. D. Willett, F. H. Jardine, I. Rouse, R. J. Wong, C. P. Landee, and M. Numata, Phys. Rev. B **24**, 5372 (1981).
[38] T. Moriya, Phys. Rev. **120**, 91 (1960).
[39] A. S. Moskvin and I. G. Bostrem, Fiz. Tverd. Tela **19**, 1616 (1977) [Sov. Phys. Solid State **19**, 1532 (1977)].
[40] F. Keffer, Phys. Rev. **126**, 896 (1962).
[41] M. V. Eremin, in *Spektroskopiya Kristallov*, edited by A. A. Kapliyanski (Nauka, Leningrad, 1965).
[42] L.-P. Regnault, I. A. Zaliznyak, and S. V. Meshkov, J. Phys.: Condens. Matter **5**, L677 (1993).
[43] A. I. Smirnov, T. A. Soldatov, K. Yu. Povarov, and A. Ya. Shapiro, Phys. Rev. B **91**, 174412 (2015).
[44] O. Golinelli, Th. Jolicoeur, and R. Lacaze, J. Phys.: Condens. Matter **5**, 7847 (1993).
[45] A. I. Smirnov, V. N. Glazkov, T. Kashiwagi, S. Kimura, M. Hagiwara, K. Kindo, A. Ya. Shapiro, and L. N. Demianets, Phys. Rev. B **77**, 100401(R) (2008).